**Peer Reviewed**

**Title:**
A physically-based approach for lens flare simulation

**Author:**
Keshmirian, Arash

**Acceptance Date:**
2008

**Series:**
UC San Diego Electronic Theses and Dissertations

**Degree:**
M.S., UC San Diego

**Permalink:**
http://escholarship.org/uc/item/5n07m4p6

**Local Identifier:**
b6636135

**Abstract:**
In this thesis, we present a physically-based method for the computer graphics simulation of lens flare phenomena in photographic lenses. The proposed method can be used to render lens flares from nearly all types of lenses regardless of optical construction. The method described in this thesis utilizes the photon mapping technique (Jensen, 2001) to simulate the flow of light within the lens, and captures the visual effects of internal reflections and scattering within (and between) the optical elements. The elements of the lens can be moved, as in a zoom lens, and the simulated lens flare will be modified accurately. Similarly, changes to the focus of the lens will also affect the lens flare, as would be expected in a real camera. The techniques described can be incorporated into an existing rendering engine without interfering with image generation. All new effects produced can be added upon existing output, and such an overlay maintains physical correctness as lens flares are produced through light paths not previously considered. We present images produced with our technique alongside unoptimized rendering times. At the conclusion of the thesis, we outline the limitations of our method and offer approaches to accelerate the simulation, as well as propose future work in this area

UNIVERSITY OF CALIFORNIA, SAN DIEGO

**A Physically-Based Approach for Lens Flare Simulation**

A thesis submitted in partial satisfaction of the requirements for the degree
Master of Science

in

Computer Science

by

Arash Keshmirian

Committee in charge:

Professor Henrik Wann Jensen, Chair
Professor David Kriegman
Professor Matthias Zwicker

2008

The thesis of Arash Keshmirian is approved and it is acceptable in quality and form for publication on microfilm:

_____

_____

_____
Chair

University of California, San Diego

2008

# DEDICATION

I wish to thank my parents Homa and Mansour. They bore me, brought me up, supported me, taught me, made innumerable sacrifices for me, inspired me, and loved me. To them I dedicate this thesis.

# EPIGRAPH

A technically perfect photograph can be the world's most boring picture.
—Andreas Feininger

*Andreas Bernhard Lyonel Feininger (27 December 1906 - 18 February 1999) was a French-born American photographer, and writer on photographic technique, noted for his dynamic black-and-white scenes of Manhattan and studies of the structure of natural objects.*

TABLE OF CONTENTS

Signature Page . . . . . iii

Dedication . . . . . iv

Epigraph . . . . . v

Table of Contents . . . . . vi

List of Figures . . . . . viii

Acknowledgements . . . . . ix

Abstract of the Thesis . . . . . x

Chapter 1. Introduction . . . . . 1

Chapter 2. Background . . . . . 4
2.1 The Lens Flare . . . . . 4
2.2 Related Work . . . . . 8

Chapter 3. Modeling Lenses . . . . . 10
3.1 Measurements . . . . . 10
3.2 Modeling Lenses Using CSG Primitives . . . . . 11
3.2.1 Choosing a Modeling Approach . . . . . 11
3.2.2 Modeling Lenses . . . . . 13
3.3 Housing and Camera . . . . . 16

Chapter 4. Rendering Lenses . . . . . 19
4.1 Rendering Lens Elements . . . . . 19
4.1.1 Glass-Glass Interfaces . . . . . 21
4.2 Photon Mapping . . . . . 22
4.2.1 Density Estimation of the Image Sensor Photon Map . . . . 23
4.3 Light Sources . . . . . 24
4.3.1 Photon Emission . . . . . 24
4.4 Scattering Effects . . . . . 25
4.4.1 Internal Surface Scattering . . . . . 26
4.4.2 Dust and Grease Accumulation . . . . . 26
4.4.3 Glass Scattering . . . . . 26
4.5 Rendering . . . . . 27

Chapter 5. Results . . . . . 28
5.1 Lenses . . . . . 28
5.2 Parameters . . . . . 28
5.3 Rendered Images . . . . . 29
5.3.1 Rendered Flares from Varied Light Positions . . . . . 29
5.3.2 Rendered Flares with Varied Bounce Limits . . . . . 33
5.3.3 Rendered Flares with Massive Photon Quantities . . . . . 35
5.4 Photographic Examples . . . . . 38
5.4.1 Canon EF 70-200mm $f/2.8$**L** . . . . . 38
5.5 Discussion of Results . . . . . 39

Chapter 6. Future Work . . . . . 41
6.1 A Complete Simulation of Lens Flare . . . . . 41
6.1.1 Wave Effects . . . . . 41
6.1.2 Coatings . . . . . 42
6.2 Improving the Speed of Lens Flare Simulation . . . . . 42

References . . . . . 44

LIST OF FIGURES

Figure 1.1: Lens flare . . . . . 2

Figure 2.1: Lens flare . . . . . 5
Figure 2.2: Ghost distribution . . . . . 6
Figure 2.3: Anti-reflection coating . . . . . 8

Figure 3.1: Double-Gauss Lens 1 . . . . . 11
Figure 3.2: Double-Gauss Lens 2 . . . . . 14
Figure 3.3: Convex-Concave Lens Element . . . . . 15
Figure 3.4: Convex-Convex Lens Element . . . . . 16
Figure 3.5: Image Sensor . . . . . 17
Figure 3.6: Lens Cutaway . . . . . 18

Figure 4.1: Angle Diagram . . . . . 21

Figure 5.1: Rendering Scene Setup . . . . . 29
Figure 5.2: Synthetic 80-200mm Flare 1 . . . . . 30
Figure 5.3: Synthetic 80-200mm Flare 2 . . . . . 31
Figure 5.4: Synthetic 80-200mm Flare 3 . . . . . 32
Figure 5.5: Synthetic 80-200mm Flare 4 . . . . . 32
Figure 5.6: 2-Bounce Flare . . . . . 33
Figure 5.7: 5-Bounce Flare . . . . . 34
Figure 5.8: 10-Bounce Flare . . . . . 34
Figure 5.9: High Quality Flare 1 . . . . . 35
Figure 5.10: High Quality Flare 2 . . . . . 36
Figure 5.11: High Quality Flare 3 . . . . . 36
Figure 5.12: High Quality Flare 4 . . . . . 37
Figure 5.13: Photographic Telephoto Flares . . . . . 38
Figure 5.14: Ray Paths . . . . . 40

ACKNOWLEDGEMENTS

I want to greatly acknowledge my advisor Dr. Henrik Wann Jensen for giving me the start I needed to realize my dream of working in image synthesis. His enthusiasm for physically-based simulation (even when it involves savage amounts of brute force) is contagious, and his support in my research has been valuable.

Dr. Matthias Zwicker provided me with a few energetic pushes along the way in this adventure, and for those I am very thankful.

I want to thank Dr. David Kriegman for reading this thesis on an extremely tight schedule, an effort I greatly appreciate.

I want to thank Wojciech Jarosz for his help in verifying some of the finer points of light transport, and for his moral support when it was hard to see the light at the end of the tunnel.

I want to thank Dana Dahlstrom for putting together the UCSD Thesis Template for LaTeX; it was immeasurably helpful in producing this document, and it saved me many hours in the formatting process.

I also want to thank Karl Gumerlock at Stanford University for generously providing processing resources for many of the renderings in this paper.

ABSTRACT OF THE THESIS

**A Physically-Based Approach for Lens Flare Simulation**

by

Arash Keshmirian
Master of Science in Computer Science
University of California, San Diego, 2008
Professor Henrik Wann Jensen, Chair

In this thesis, we present a physically-based method for the computer graphics simulation of lens flare phenomena in photographic lenses. The proposed method can be used to render lens flares from nearly all types of lenses regardless of optical construction.

The method described in this thesis utilizes the photon mapping technique (Jensen, 2001) to simulate the flow of light within the lens, and captures the visual effects of internal reflections and scattering within (and between) the optical elements. The elements of the lens can be moved, as in a zoom lens, and the simulated lens flare will be modified accurately. Similarly, changes to the focus of the lens will also affect the lens flare, as would be expected in a real camera.

The techniques described can be incorporated into an existing rendering engine without interfering with image generation. All new effects produced can be added upon existing output, and such an overlay maintains physical correct-

ness as lens flares are produced through light paths not previously considered. We present images produced with our technique alongside unoptimized rendering times. At the conclusion of the thesis, we outline the limitations of our method and offer approaches to accelerate the simulation, as well as propose future work in this area.

# Chapter 1.

# Introduction

The perceived realism of rendered images depends on the accurate simulation of materials, environmental effects, cameras, and lighting. The often-colorful flare produced by a photographic lens when capturing scenes with particularly bright light sources occurs frequently in photographic images, yet historically little effort has been made to develop physically-based techniques for the simulation of this phenomenon. Popular methods for producing lens flare effects employ artistic representations or rudimentary non-physical simulations. These techniques not only fall far short of realism, but have also given the lens flare a reputation as a notoriously clichéd and cheesy element to be avoided in renderings and artwork. Unfortunately, avoiding the simulation of the lens flare entirely is a solution adopted by many, but this brings about an unrealism of its own; light sources such as the sun are represented merely by a white circle, and the headlights of an oncoming car similarly lose the drama they might have were they shot on film. Thus, it is clear that an accurate simulation of lens flares is destined to be of great use in many virtual scenes, and completely mandatory in others.

The solution we propose in this thesis aims to reproduce the effect by more accurately simulating light flow at the source of the flare: the lens. The

Figure 1.1: A lens flare adds drama and focus to this scene. *David Beckstead*

lens flare itself has a complex structure produced by many different properties of the optical lens. This thesis aims to capture one of the most visually important features, the line of circular halos extending from the light source on an axis (Figure 1.1). The other subtle features of the flare, such as dispersion effects and digital sensor diffraction are left for future work.

Our solution begins with an accurate modeling of the optical elements of the lens and the materials used in the design. It is not uncommon for lenses to be designed with many different materials for the optical elements, each with different characteristics. Fortunately, the specifications for these materials are widely available. Any lens can be modeled for this method, so long as specifications are available for the curvatures, spacing, and materials. There are a few exceptions for some exotic lenses, and these will be discussed in more detail later on in this text. The modeling step in this paper is similar to that used by Kolb et al. (1995).

Once the lens is modeled, a photon mapping approach is used to trace the flow of light into the lens and onto the sensor plane behind the lens. The source of the photons can be any element in the scene for which lens-flare simulation is desired. When the photon tracing pass is complete, and photons from

non-image-forming paths are stored, density estimations are performed on the sensor plane to reveal the lens flare. Post processing steps discussed in more detail in the text can be used to further clarify the flare. The flare is obtained can be overlaid directly upon an image rendered through normal means, and this will add further completeness to the rendering solutions accuracy.

# Chapter 2.

# Background

## 2.1 The Lens Flare

The term *lens flare* (also referred to more generally as *veiling glare*) is commonly used by photographers and videographers to describe the phenomena observed when a camera is subjected to a light source which is significantly brighter than the rest of the scene. The appearance of the phenomena observed can vary significantly from lens to lens and camera to camera. However, the major features of the effect are similar in most cases, and here we will describe them.

At the location of the center of the flare, where the source is located, several effects originate (Figure 2.1). The most prominent of these is often a series of bright lines or streaks radiating outward from the source to form a star-shaped effect. In addition to this effect, a less distinct glare is also sometimes present. This glare appears as a bright region around the source which fades gradually away from the source. The contrast of the image is visibly reduced when this glare is particularly strong, and it can sometimes extend over the entire frame. The image is often described as washed-out in these cases. This glare is commonly seen on inexpensive equipment such as disposable cameras (as a result

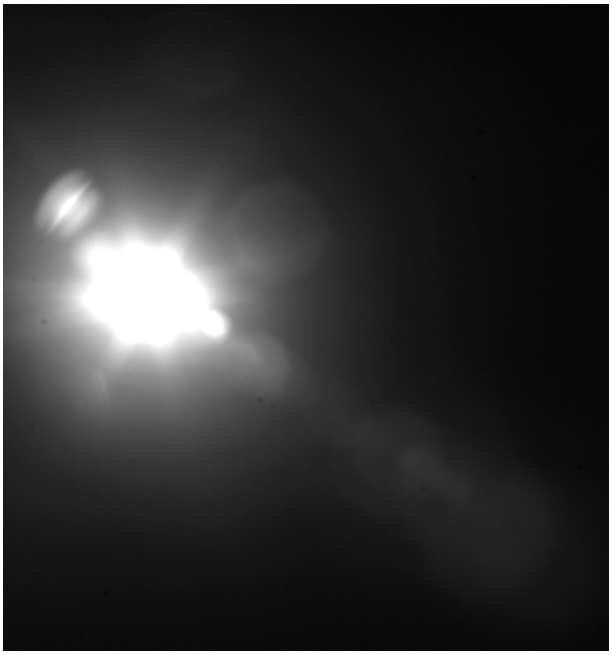

Figure 2.1: A lens flare caused by the sun. Canon EOS 20D, EF 70-200mm $f/2.8\mathbf{L}$

of inferior optics), and is often the cause of bad sunny day on the beach photos. The contrast given by the useful light, also known as the "ideal contrast", is given by

$$K' = \frac{I_{\text{max}} - I_{\text{min}}}{I_{\text{max}} + I_{\text{min}}}.$$

The intensity of veiling glare $I_0$ is added equally to $I_{\text{min}}$ and $I_{\text{max}}$, so the contrast is reduced in the real contrast $K''$:

$$K'' = \frac{I_{\text{max}} - I_{\text{min}}}{I_{\text{max}} + I_{\text{min}} + 2I_0}.$$

The ratio between real contrast and the ideal (Franke, 1966, p63) is

$$K''/K' = \frac{I_{\text{max}} + I_{\text{min}}}{I_{\text{max}} + I_{\text{min}} + 2I_0} \approx 1 - \frac{2I_0}{I_{\text{max}} + I_{\text{min}}}.$$

The other major feature present in lens flares, which is the focus of this thesis, is the series of circles or rings in the image. These phenomena, which we

will refer to as *ghosts*, lie on an axis which crosses from the source of the flare through the center of the frame. The number and position of the circular ghosts depends on the construction of the lens, as well as its deflection from the source, that is, the angle between the optical axis of the lens and the line from the lens to the flare source. As the angle decreases and the lens comes to point into the source, the circular ghosts are brought closer together.

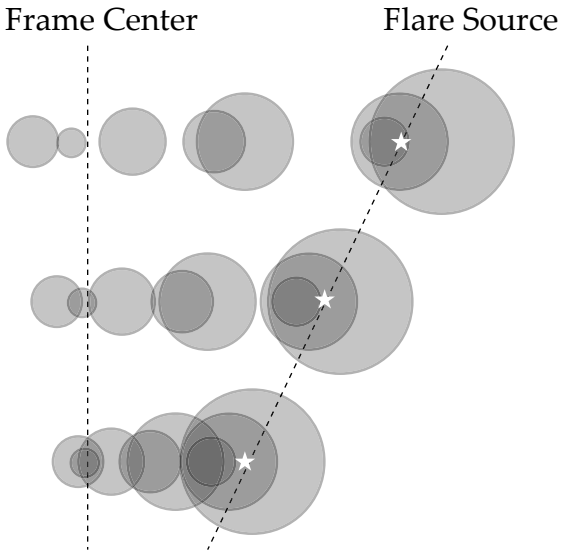


Figure 2.2: An illustration of the distribution of ghosts as the separation between the source and the center of the frame changes.

The cause of these circular ghosts is light coming to the sensor / film along non-image-forming paths. Image-forming paths are paths where the light passes through the lens interfaces with no reflection. At each interface, image-forming light is refracted and travels sequentially through the elements of the lens until it reaches the photosensor. In practice, however, light will reflect at interfaces as well, following more complex paths before it finally reaches the photosensor. It is this light which produces the ghost patterns, and they are essentially reflections of the lens elements themselves. The number of interfaces present in the lens can be used to find the number of potential reflections cast

on the photosensor with the following series:

$$\begin{aligned} R &= (2M-1) + (2M-2) + (2M-3) + \cdots + 1 \\ &= M(2M-1) \\ &= 2M^2 - M. \end{aligned}$$

Here $R$ is the number of reflections possible, and $M$ is the number of optical groups with air-to-glass interfaces $2M$. This is the upper limit on the number of ghosts present in the lens flare (Koren, 2007). In reality, reflections from every possible surface are not usually present in the flare.

Lens designers have developed many techniques to combat lens flare, the simplest of which is the lens hood. Hoods are a simple plastic or metal fitting for the front of the lens which block light from entering into the lens from outside the field of view. The inside of these hoods are sometimes covered with black flocking to absorb light that might reflect from the interior of the hood, further blocking unwanted light. Within the lens, coatings are used to limit the reflectivity of the lens surfaces. Uncoated glass is noted to have an average reflectivity of around 4%, whereas a single-layer coated optic cuts that reflectivity to 2%. More advanced techniques such as multi-coating can limit reflectivity further to as low as 0.25% (Smith, 2000, page 205). Coatings work by producing destructive interference. Light is partially reflected from the coating surface and from the glass surface, with the coating thickness equal to some fraction of the wavelength to be cancelled (Figure 2.3). This causes reflected light to cancel itself out, and multi-coating approaches are able to cancel reflections across a range of wavelengths.

This technology is frequently used in other optical glass as well, such as eyeglasses, display windows, and framing glass. The side-effect of these anti-reflective coatings is the color they impart on the reflections that remain; ghosts from coated lenses are seen in a variety of pinks, greens, and blues whereas the ghosts from uncoated lenses are usually similar to the color of the source. While

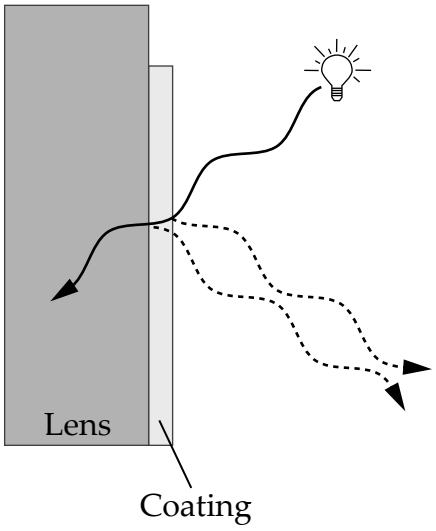


Figure 2.3: A single-layer coating reflects and cancels incoming light of a specific wavelength. Multiple coatings are often used to provide defense against a range of wavelengths.

we did not simulate this effect in this thesis, it is not complex to extend the methods described to account for coatings. Assuming that no coatings are applied, the percentage of light reflected can be computed (based on the properties of the lens material) using the *Fresnel reflection coefficient*.

This forms the foundation for how we compute light paths within the optics of the lens. The more intimate details of the light transport are elucidated later in the thesis.

## 2.2 Related Work

This thesis draws primarily from the work of Kolb et al. (1995), and follows their notion of rendering using a realistic camera model. We do not render the image itself through the lens as in their work, but rather use the lens to model light flow onto the camera sensor to visualize the lens flare pattern.

While it is certainly possible to incorporate the rendering approach described by the authors with our method for a more complete solution, our emphasis is on rendering the lens flare itself. This paper was also very helpful in finding a source (Smith, 2005) for accurate numerical measurements of lenses, and served as a useful guide to their interpretation.

Late in the development of this thesis, we came across the work of another student (Chaumond, 2007) who used an approach similar to ours for rendering lens flares, but instead of photon-mapping, approached the problem with a pure path-tracing approach. Chaumond also surmised that Mie scattering may play a role in the light flow through lenses, and this gave us further cause to explore this in our research.

# Chapter 3.

# Modeling Lenses

## 3.1 Measurements

In order to meet our goal of modeling a lens accurately, it is necessary to first have an accurate source of measurements for the lens. This can often pose a challenge when a specific lens is desired, as most lens designs are closely guarded by their designers and manufacturers. In our research we tried to find measurements for lenses from Canon, to no avail. However, many lens designs follow common forms, such as the Heliar, Tessar, Cooke-Doublet, and so on. General examples of these lenses are widely available, and we found Smith (2005) to be a particularly good source of these examples.

Measurements for lenses (as shown in Figure 3.1) are commonly presented in a standard format. At the right is a schematic of the lens, with the lens looking to the left. Alongside the schematic for the lens is a table containing the measurements of the lens. Each row represents a surface (with the exception of the sixth, which is the aperture) of the lens. This includes glass-glass interfaces. The first column of the table gives the curvature of the surface, as a radius of the sphere with the same curvature. Negative values in this column represent surfaces that are oriented in the opposite direction. The second column gives

| radius | thick | $n_d$ | V-no | ap |
|---|---|---|---|---|
| 58.950 | 7.520 | 1.670 | 47.1 | 50.4 |
| 169.660 | 0.240 | | | 50.4 |
| 38.550 | 8.050 | 1.670 | 47.1 | 46.0 |
| 81.540 | 6.550 | 1.699 | 30.1 | 46.0 |
| 25.500 | 11.410 | | | 36.0 |
| | 9.000 | | | 34.2 |
| -28.990 | 2.360 | 1.603 | 38.0 | 34.0 |
| 81.540 | 12.130 | 1.658 | 57.3 | 40.0 |
| -40.770 | 0.380 | | | 40.0 |
| 874.130 | 6.440 | 1.717 | 48.0 | 40.0 |
| -79.460 | 72.228 | | | 40.0 |

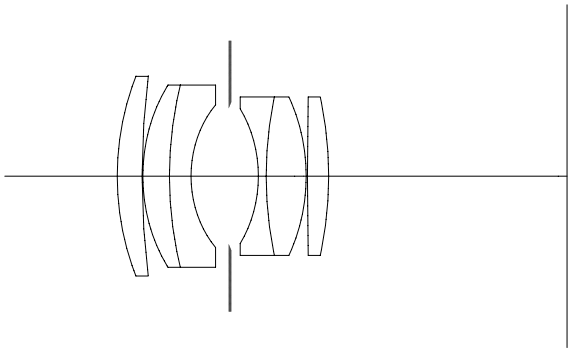

Figure 3.1: An example of a schematic for a Double-Gauss lens. (Smith, 2005, page 312)

the distance between the center of the surface and the center of the next surface. The third column gives the index of refraction for light at 587.6 nm. The fourth column is the *V-number*, which is a measure for the amount of *dispersion* the material produces. Dispersion represents the rate of change in index of refraction as the wavelength changes. The last column is the diameter of the surface. We use these measurements as a guide for building our lenses using the *constructive solid geometry* (CSG) technique described in the next section.

## 3.2 Modeling Lenses Using CSG Primitives

### 3.2.1 Choosing a Modeling Approach

There are many approaches for modeling the optical surfaces within a lens, each with its own advantages. For our simulation, we desired a system that is highly accurate in representing the surfaces of the lenses, and is computationally cheap to intersect with. The following is a comparison of techniques we considered:

**Polygon Modeling** The fastest approach for modeling surfaces is to avoid di-

rectly modeling them in the rendering engine, and to instead use a modeling application such as 3D Studio Max or Maya[1]. After the lens is modeled it is imported into the engine as a triangle mesh. The advantage of this technique is that it requires little implementation on the part of the programmer, but is faced with accuracy issues. In order for the lenses to be reasonably smooth, the triangle meshes involved must be extremely dense. Even so, the lens surfaces will remain faceted, and barycentric interpolation must be used to smooth the faces. The intersection costs of using dense triangle meshes, coupled with concerns over accuracy led us not to use this method.

**Surfaces of Revolution** Surfaces of revolution, such as those involving a Bézier spline revolved around an axis to produce a surface, are an alternative to a triangle representation. These surfaces have infinite precision as they are parametric, but there are two drawbacks. The first is that intersections with such a surface are still slightly expensive. Second, the surfaces of lenses (with the exception of *aspherical* lenses, which are not particularly common) are spherical. This is an issue because of the well-known caveat that Bézier curves cannot represent perfect circles[2]. An approach that produces imperfect circles was not in line with our requirements.

**Constructive Solid Geometry** CSG Modeling involves creating lens optics with boolean operations with various primitives. In the case of lenses, it is sufficient to use spheres and cylinders of various sizes. The CSG approach allows for infinite precision on geometry, as the spherical surfaces remain

[1] 3D Studio MAX and Maya are registered trademarks of Autodesk Corporation.

[2] This in itself is a particularly interesting problem as many drawing formats, such as PostScript, support only Bézier curves and not parametric circles. The problem of representing circles is best overcome with an approximation for $\kappa$, the length of the tangential Bézier handles at the edges of the quadrants of the circle. The approximation is $\kappa = r * 4\frac{\sqrt{2}-1}{3}$ where $r$ is the radius of the circle. This value for $\kappa$ is derived cleanly alongside figures by G. Adam Stanislav at *http://www.whizkidtech.redprince.net/bezier/circle/kappa*.

parametric. The cost of intersections is also low, as there is only a small premium incurred in addition to the cost of the component primitives, which amount to two or three per optical element. Furthermore, the CSG approach fits well with the format of lens measurements, and we will cover this in greater detail in the next section. Given these advantages and a lack of drawbacks, we elected to use CSGs for our simulation.

### 3.2.2 Modeling Lenses

The CSG system we implemented supports Subtraction, Union, and Intersection operations. We implemented these operations as nodes in a binary tree, allowing them to be nested. For example, the object equivalent to $A-(B+C)$ is simply constructed by subtracting $A$ from a union of $B$ and $C$. The implementations are fairly standard, and are summarized below, within the context of a ray tracer.

**Union ($A+B$)** The ray intersections of all sub-objects are found, and the closest one is returned.

**Subtraction ($A-B$)** The ray intersections of all sub-objects are found, and the closest of the following types of ray intersections is returned: ray intersection of $A$ which is outside $B$; ray intersection of $B$ which is inside $A$. It should be noted that if the intersection is of the second category, the normal must be reversed.

**Intersection ($A \cap B$)** The intersections of all sub-objects are found, and the closest of the following types of ray intersections is returned: ray intersection of $A$ which is inside $B$; ray intersection of $B$ which is inside $A$.

Now that the building blocks of CSG are established, we will concern ourselves with the actual construction of lens elements of various types. In prac-

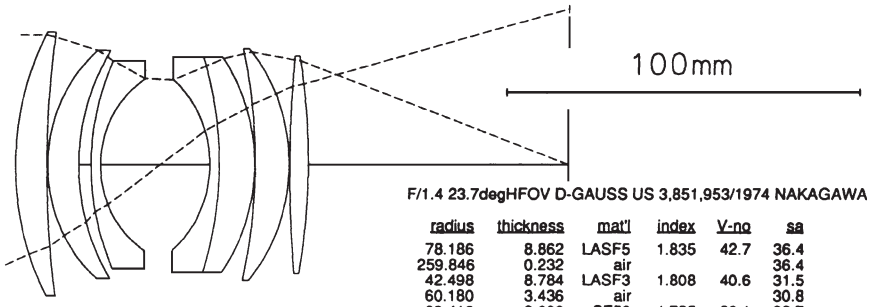


F/1.4 23.7degHFOV D-GAUSS US 3,851,953/1974 NAKAGAWA

| radius | thickness | mat'l | index | V-no | sa |
|---|---|---|---|---|---|
| 78.186 | 8.862 | LASF5 | 1.835 | 42.7 | 36.4 |
| 259.846 | 0.232 | air | | | 36.4 |
| 42.498 | 8.784 | LASF3 | 1.808 | 40.6 | 31.5 |
| 60.180 | 3.436 | air | | | 30.8 |
| 69.416 | 2.606 | SF56 | 1.785 | 26.1 | 28.7 |
| 28.654 | 16.888 | air | | | 23.7 |
| | 14.000 | air | | | 23.6 |
| -31.582 | 2.646 | SF56 | 1.785 | 26.1 | 23.5 |
| -99.808 | 9.982 | LASF3 | 1.808 | 40.6 | 29.7 |
| -52.702 | 0.192 | air | | | 29.7 |
| -150.994 | 9.692 | LAK8 | 1.713 | 53.8 | 31.9 |
| -50.290 | 0.232 | air | | | 31.9 |
| 338.224 | 5.174 | LAK8 | 1.713 | 53.8 | 30.0 |
| -186.406 | 73.796 | air | | | 30.0 |

Figure 3.2: A schematic for a Double-Gauss (Biotar) lens. (Smith, 2000, page 537)

tice, there are a limited variety of element types in lens design. Generally, an element has two spherical surfaces, and these are connected by cylindrical walls. The surfaces of the optic are of varying spherical radii, and can be convex or concave relative to the cylinder. In some designs flat "cap" surfaces are present, but this is not as common. To differentiate and clarify the various categories of elements, we will analyze the components of the lens in Figure 3.2. First, we must clarify our terms. The "back" surface of an element is the one on the right side, and the "front" is on the left. The lens, as in Figure 3.1, is looking to the left. We will progress through the elements from left to right as we describe the elements. The first element is a *convex-concave* element (see Figure 3.3). It is produced by creating a cylinder primitive that reaches the edges of both surfaces, and intersecting it with the sphere that forms the front surface. The rear surface sphere is then subtracted from this solid. The second and third are produced in the same way. It should be noted that the radius of the back surface on the third element is smaller than the radius of the cylinder from which it is cut, leaving behind a donut-shaped flat cap. Between the third and fourth elements lies the

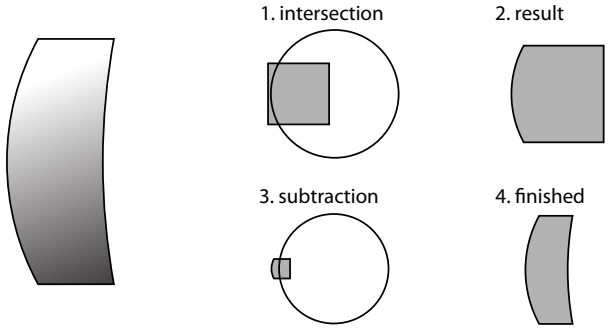


Figure 3.3: This diagram illustrates the CSG operations involved in producing a Convex-Concave lens element.

*aperture diaphragm*. We produce the aperture diaphragm by creating a cylinder[3] of large radius and minimal height, from which we subtract the aperture hole, with a cylinder of smaller radius. Continuing through the lens, the fourth, fifth, and sixth elements are *concave-convex*, and are created similarly to the first three, but in reverse order—the front surface is subtracted from the cylinder first, and then this is intersected with the rear sphere to make the rear surface. The final rear element is a *convex-convex* element (see Figure 3.4). It is produced by the intersection of the front sphere and the cylinder, the result of which is intersected with the rear sphere.

Using this technique, it is possible to represent nearly all of the lenses presented in Smith (2005). There are a few notable exceptions. The first, are aspherical lenses. These lenses have elements with surfaces that are aspherical, allowing for better distortion correction, and minimization of chromatic aberration. However, these elements are expensive to produce, and are thus significantly rarer than their spherical counterparts, and even then, only one or two elements are aspherical in a high-end lens design. It should be possible to simu-

[3] Any shape can be used for the hole; the multi-bladed aperture diaphragms of most lenses are hexagonal or octagonal. Only a few (very expensive) camera lenses have circular apertures over any appreciable range of aperture sizes.

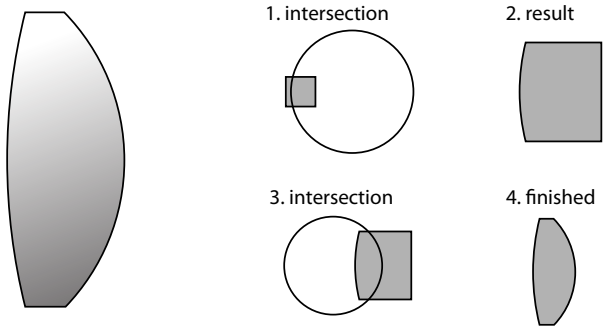


Figure 3.4: This diagram illustrates the CSG operations involved in producing a Convex-Convex lens element.

late these as needed with surfaces of revolution as described in 3.2.1. The other form of lens not directly considered by this thesis are catadioptric[4] lenses, which consist of both optics and mirrors. While we did not explore these lenses in this thesis, it should be possible to construct them in a similar manner to dioptrics by using CSG or surfaces of revolution, and simulating a mirrored material for the surfaces instead of a dielectric, as we discuss in the next chapter.

## 3.3 Housing and Camera

Once elements are modeled, they are set into geometry that represents the housing of the lens, as well as the camera itself. The detail involved in the housing can be as simple as a tube into which the elements are placed, and this is often sufficient. However, in some designs where light may leak around elements, it is necessary to surround them more closely within the lens, as in real

[4]This design is used often in very compact, inexpensive super-telephoto lenses, which, while inferior in terms of optical quality, are often significantly more practical than the dioptric (purely refracting) alternative. For example, a Russian-made catadioptric 1200mm telephoto can be found for under US$400, and weighs less than a pound, whereas the Canon glass-equivalent is sold at around US$85,000 and weighs over 30 lbs. Catadioptric lenses are popular with bird-watchers and wilderness photographers for whom weight and cost far outweigh the immediate differences in image fidelity.

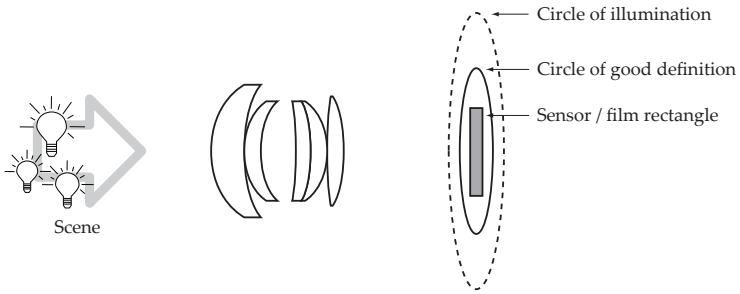


Figure 3.5: A diagram of the image sensor, as positioned within the illumination circle.

life lenses (see the cutaway shown in Figure 3.6). Furthermore, the effect of light bouncing off of the inside of the front of the lens can be simulated if the housing model is sufficiently detailed. The interior of the camera filmbox can be simulated with precision if necessary, and it is possible to capture mirror reflections in this way. In our experiments, we approximate the filmbox with a dark box. At the rear of the box, we place the image sensor (Figure 3.5) to capture the incoming light. The function of the sensor in our simulation is detailed in the next chapter.

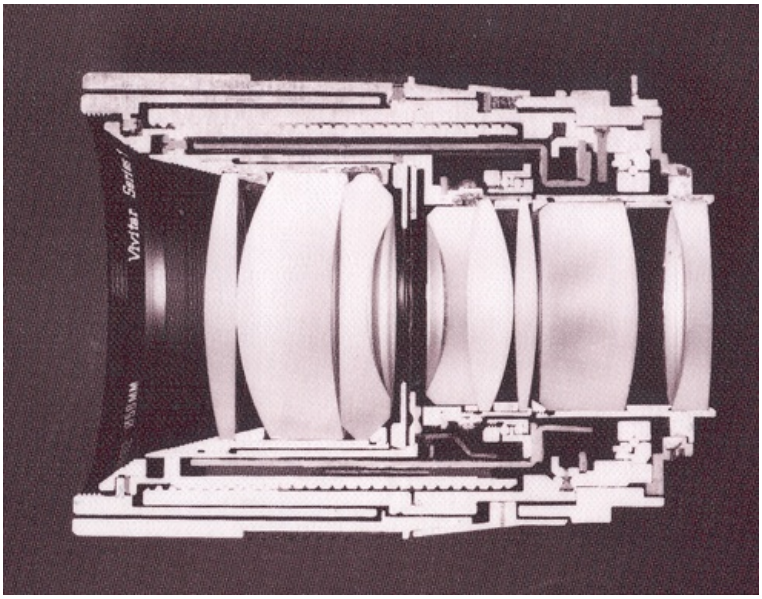


Figure 3.6: A cutaway view of the Vivitar Series 1 90mm $f/2.5$ (Kingslake, 1992, cover)

# Chapter 4.

# Rendering Lenses

After the lens is modeled using the approach described in Chapter 3., we set up a simple scene with a light source, and the lens-camera assembly. This chapter details the processes involved in rendering a lens flare from this setup. In the first section, we examine the behavior of light at air-glass and glass-glass interfaces, and then go on in the next section to describe the light sources we used. Following that section, we elaborate the photon mapping approach that lies at the core of our technique, and we finish the chapter with a look at simulating the subtle scattering of light within the lens and its optical elements.

## 4.1 Rendering Lens Elements

There are two types of surfaces with which we are chiefly concerned in this simulation: air-glass interfaces, which occur on the front and back side of each individual element, and glass-glass interfaces, which occur when two elements are cemented together optically. Simulating the physics of reflection and refraction at these surfaces is crucial for accurate photon flow when we perform our photon tracing later in the chapter.

When a photon trace ray intersects an interface, we must determine the

following quantities:

1. The amount of light reflected from the surface, as a percentage of incoming light
2. The direction[1] of light reflected from the surface
3. The amount of light refracted by the surface, as a percentage of incoming light
4. The direction of light refracted by the surface

We will first concern ourselves with the directional quantities. We assume the lens surfaces to be perfectly smooth, and thus, we can determine the specular reflection $\vec{\omega}_s$ in the mirrored direction:

$$\vec{\omega}_s = \vec{\omega}' - 2\left(\vec{\omega}' \cdot \vec{n}\right)\vec{n}, \tag{4.1}$$

where $\vec{n}$ is the surface normal and $\vec{\omega}'$ is the incoming ray direction. The direction of light refracted depends on the index of refraction (IOR) $\eta_1$ of the surrounding air (or, in the case of glass-glass interfaces, of the preceding element) and the IOR $\eta_2$ of the element to be entered. We can determine the direction of the refracted ray by *Snell's law*:

$$\vec{\omega}_r = -\frac{\eta_1}{\eta_2}((\vec{\omega} \cdot \vec{n})\vec{n} - \vec{\omega}) - \left(\sqrt{1 - \left(\frac{\eta_1}{\eta_2}\right)^2 (1 - (\vec{\omega} \cdot \vec{n})^2)}\right)\vec{n}. \tag{4.2}$$

The *Fresnel equations* give the amount of parallel-polarized and orthogonally-polarized (with reference to the plane of incidence) light reflected as a ray passes from one medium to another. We can combine these to find the Fresnel reflection coefficient $F_r$:

$$F_r(\theta) = \frac{1}{2}\left(\left(\frac{\eta_2 \cos\theta_1 - \eta_1 \cos\theta_2}{\eta_2 \cos\theta_1 + \eta_1 \cos\theta_2}\right)^2 + \left(\frac{\eta_1 \cos\theta_1 - \eta_2 \cos\theta_2}{\eta_1 \cos\theta_1 + \eta_2 \cos\theta_2}\right)^2\right), \tag{4.3}$$

[1] It should be noted that we will handle all reflections and refractions as purely specular in this section. We will describe potential extensions to this model in Section 4.4.

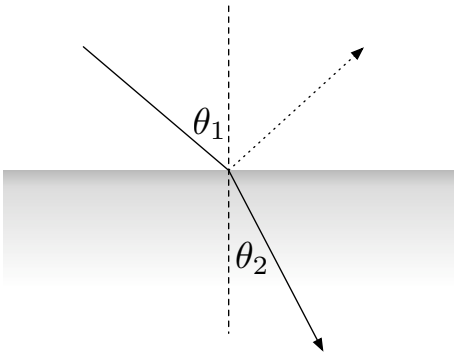


Figure 4.1: The angles used in calculating the fresnel coefficients. Reflected and refracted rays are shown.

where $\theta_1$ is the angle between the incoming ray and normal incidence, and $\theta_2$ is the angle between the exiting ray and the inside normal (see Figure 4.1. In order to determine the amount of light refracted, we can simply use $1 - F_r$. This assumes that the element absorbs zero light. In practice, with glass at the thickness of photographic lens elements, this is not an unreasonable assumption (Smith, 2005). It should be noted that an alternative approximate formulation exists for 4.4, called the *Schlick approximation*:

$$F_r(\theta) \approx F_0 + (1 - F_0)(1 - \cos\theta)^5, \tag{4.4}$$

where $F_0$ is the value of the full Fresnel coefficient when $\theta = 0$. The approximation is of course less computationally expensive than obtaining the real Fresnel coefficient, but to meet our goals for maximum accuracy, particularly with such an important computation, for this thesis we use the full fresnel equation at the expense of render times.

### 4.1.1 Glass-Glass Interfaces

In many lens designs, optical elements are cemented together, forming a direct optical interface between the two pieces of glass. This can be seen in ele-

ments four and five in Figure 3.1. The change in index of refraction between the two elements is smaller than if there were an airspace gap between the lenses. Because of the CSG approach we use to model lenses, some special care must be given to the handling of these interfaces to insure that no airspace is present.

The CSG approach we are using does not explicitly allow us to mate surfaces, as each element has a closed surface representation. However, because the material of each region in the CSG element can be individually assigned, we can use this to develop a workaround. We will use an example of the mating of two elements to describe our solution. First, we move forward the rear side of the front element by a very small amount (.01mm or so is sufficient), and assign this surface an index of refraction of 1.0. This allows paths exiting the element to leave without any deviation in course, and the small shift in position resolves any ambiguous intersections and coincidences between the two mated surfaces. Next, we assign the corresponding surface on the front of the second element an index of refraction equal to $\eta_2/\eta_1$ where $\eta_1$ and $\eta_2$ are the IORs of the two surfaces, respectively.

## 4.2 Photon Mapping

In order to determine the flow of light into the lens and onto the sensor, we use a photon mapping approach (Jensen, 2001). Photons are cast from light sources in the scene toward the camera lens, and the path of each photon is ray-traced as it interacts with the interfaces within the lens. Photons which eventually reach the image sensor at the rear of the lens are stored in the photon map. Any photons which do not reach the lens or do not reach the image sensor are not stored, and are subsequently discarded. Also, it is appropriate to discard photons that travel directly through the lens and land on the image sensor, that is, with no reflections, passing through each element sequentially. The contribution from these photons is expected to be considered by the stan-

dard rendering procedure for the base image, and is not part of the lens flare. If we include these photons, then it must be ensured that no other rendering is performed[2].

### 4.2.1 Density Estimation of the Image Sensor Photon Map

In our lens flare simulation, the photon map contains all the photons that have intersected with the image sensor plane. To determine the irradiance at each point on the sensor surface, we must perform a density estimation of the photon map. Because the surface is flat, all stored photons are planar, and this makes the density estimation simple. We enlarge a circle up to radius $r$ surrounding the point we would like to estimate, and we can determine the irradiance $E$ from the $n$ photons gathered with power $\Delta\Phi_p$ by

$$E = \sum_{p=1}^{n} \Delta\Phi_p \frac{r^2}{\pi} \quad . \tag{4.5}$$

This irradiance is then used as the amount of light contributed by the lens flare to the pixel on the image sensor. In our simulation, we assume that the sensors are omnidirectional, but due to the direction of incoming photons being nearly perpendicular to the sensor surface as they exit the rear element, this is not an issue.

It should also be noted here that the standard photon implementation utilizes a *kd-tree* for storing photons. In this simulation, all stored photons are coplanar, so a two-dimensional data structure could be used instead as an optimization.

[2]It is in fact possible to render scenes in this fashion, using only photons. To make this solution accurate, photons cast from light sources will need to interact with surfaces in the scene as they will in a standard photon mapping implementation. Some (small) percentage of those photons would enter the lens. Of course, this is generally quite impractical due to the astronomical number of photons required for a pleasing image, but pedagogically, is directly analogous to the rendering method proposed by Kolb et al. (1995).

## 4.3 Light Sources

In our simulations, we use point-based light sources. We support omni-directional sources and spotlight sources, with the latter type being used primarily for performance reasons which we will discuss later on. This approach is certainly not limited to point-sources, however, and any type of photon-casting source can be used. Lens flares from larger sources are significantly less distinct than those from point sources.

### 4.3.1 Photon Emission

We emit photons from point sources uniformly in all directions. The simplest way to do this is to generate the three components of the direction vector $\vec{d}$ for each photon by rejection sampling with three random numbers $\xi_1$, $\xi_2$, and $\xi_3$ (Jensen, 2001):

$$
\begin{aligned}
& x = \xi_1, \text{ where } \xi_1 \in [0,1], \\
& y = \xi_2, \text{ where } \xi_2 \in [0,1], \\
& z = \xi_3, \text{ where } \xi_3 \in [0,1], \\
& \quad \text{with } (x^2 + y^2 + z^2) > 1 \\
& \vec{d} =< x, y, z > .
\end{aligned}
$$

A more efficient way to generate directions is the trigonometric method, which uses two random numbers $\xi_1$, $\xi_2$, and wastes no samples, as is the problem with

rejection sampling.

$$
\begin{aligned}
z &= \xi_1, \text{ where } \xi_1 \in [-1, 1], \\
t &= \xi_2, \text{ where } \xi_2 \in [0, 2\pi], \\
w &= \sqrt{1 - z^2} \\
x &= w\cos(t); \\
z &= w\sin(t); \\
\vec{d} &= < x, y, z > .
\end{aligned}
$$

Photons cast by either method are then scaled to be an equal fraction of the total power of the light.

Because photons which do not enter the lens are not important to the lens flare solution, we can highly optimize the number of photons required for an accurate lens flare by emitting only the photons which are expected to enter the lens. This can be done in a number of ways, the simplest of which is to only emit photons in the direction along the smallest cone that intersects the front element of the lens. In situations where the light source is far away from the lens, the improvements gained by this approach are quite significant.

## 4.4 Scattering Effects

There are a number of sources for scattering within the lens, and these can affect the lens flare. These sources will contribute to the overall veiling glare present, but do not generally add any distinct features. However, in this section we will discuss these sources, as their simulation may be appropriate in some circumstances.

### 4.4.1 Internal Surface Scattering

The internal surfaces of the barrel of the lens can contribute diffuse scattering to the light flow within the lens. In many lenses these surfaces are painted a highly non-reflective flat black, or in higher quality optics, coated with a black flocking material to further absorb light. A situation where these surfaces might make a more significant contribution are in extremely cheap optics where a black colored plastic is used for the lens body (Kingslake, 1992, p133), such as in toy telescopes, disposable cameras, and some cellular telephone cameras. The reflectance of plastic can be particularly high at glancing angles, and this incidence is common within a lens.

### 4.4.2 Dust and Grease Accumulation

The outer element of a lens (or if present, the filter on the lens) is a prime location for the accumulation of dust, grease, and other environmental contaminants. Depending on the degree of build-up on the surface of the glass, significant glare from scattering can be observed (Kingslake, 1992, p133). In addition to glare, severe contamination can result in blurring of the image formed by the lens.

### 4.4.3 Glass Scattering

Imperfections in the glass elements themselves can also scatter light. These imperfections are a result of voids or bubbles in the glass, as well as microscopic cracks formed during the annealing and cooling of the element during its manufacture. In addition, the cemented doublets in some lenses can cause scattering due to imperfections in the optical cement and in the interface between the two lenses. These scattering effects can likely be modeled and approximated using Mie theory (Marston et al., 1981).

## 4.5 Rendering

Once the photon map has been filled with the photons from the lens flare, rendering of the flare can be performed. Assuming the aspect ratio of the camera sensor and the final image are the same, a direct mapping between the image pixels and locations on the sensor can be found. Density estimations at those pixel locations will yield the image of the flare recorded by the sensor. Rendering the image in this way is fast, but requires some special implementation within a standard raytracer. An alternative to this method is to raytrace the surface of the sensor directly, using an orthographic projection. This method is more computationally costly, but may be the most straightforward way to implement this technique in some systems

Once the final lens flare image $\mathbf{I}_f$ is rendered, the lens flare can then be overlaid additively upon an image rendered using standard methods $\mathbf{I}_s$ to find the total image $\mathbf{I}_t$:

$$\mathbf{I}_t = \mathbf{I}_f + \mathbf{I}_s.$$

It should be noted that due to the high accuracy of our method in reproducing distortions and spherical aberrations in the lenses represented, the standard method needs to also take these into account in order for the overlay to be correct. That is, if these distortions are not considered, the source of the lens flare may be displaced significantly between the two images, especially in situations where wide FOV lenses are used and the source is toward the edge of the frame. In situations where the lens distortion is not significant, there may be no perceptible need for correction.

# Chapter 5.

# Results

In this chapter we display some of the renderings produced in our tests. For comparison, at the end of the chapter we also provide photographic examples that approximate the conditions simulated.

## 5.1 Lenses

For our tests we modeled the Nikon 80-200mm $f/2.8$ (Smith, 2005), which we fix at 80mm.

## 5.2 Parameters

To produce these renderings we cast photons originating from a point source 3.6M in front of the lens (Figure 5.1). The photons are aimed toward the front element of the lens, and based on empirical adjustments, the direction and spread of these photons were tuned to minimize photon loss. On average, approximately 30-32% of cast photons reach the sensor. The remaining photons are either absorbed by internal black surfaces of the lens, or are reflected out of the lens.

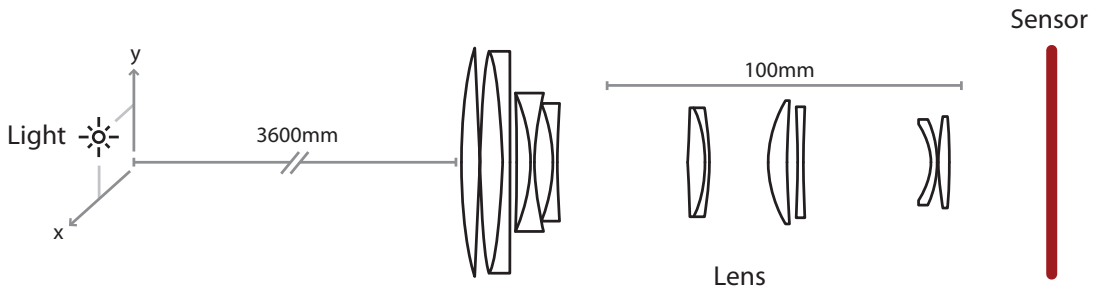


Figure 5.1: The scene setup for the renderings in this section.

## 5.3 Rendered Images

The images contained in this section have been brightness and contrast-enhanced to improve visibility in printed form.

### 5.3.1 Rendered Flares from Varied Light Positions

The images in this section were rendered on an Apple MacBook Pro with a 2.33GHz Intel Core 2 Duo processor. In all images, 10 million photons were cast.

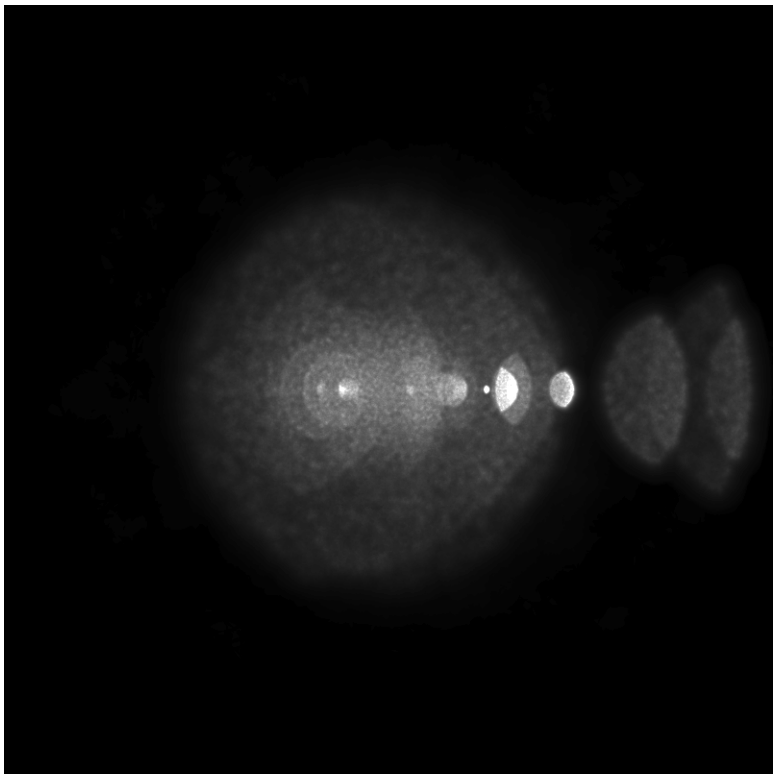

Figure 5.2: A synthetic flare. Light source position: $x = -600$mm, $y = 0$mm. Rendering time: 7867 sec.

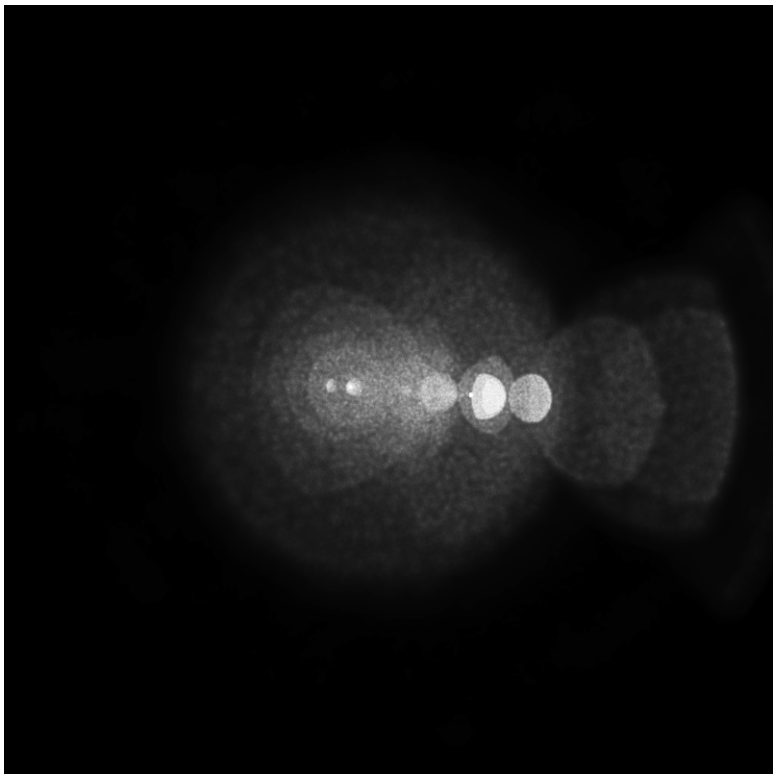

Figure 5.3: A synthetic flare. Light source position: $x = -500$mm, $y = 33$mm. Rendering time: 8586 sec.

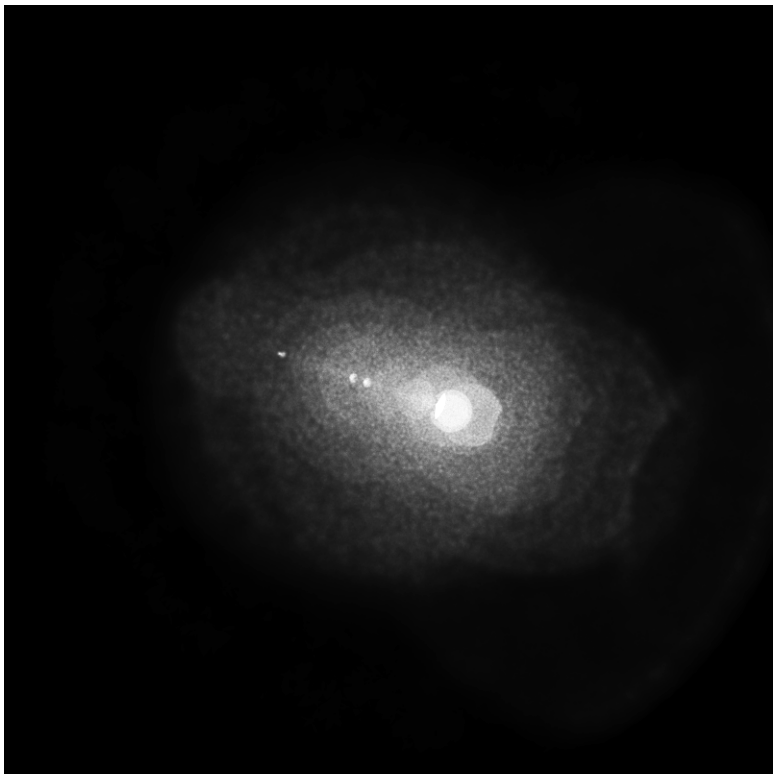

Figure 5.4: A synthetic flare. Light source position: $x = -300$mm, $y = 99$mm. Rendering time: 8943 sec.

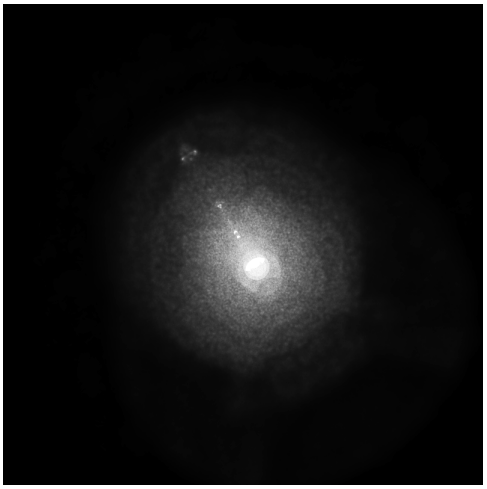

Figure 5.5: A synthetic flare. Light source position: $x = -100$mm, $y = 165$mm. Rendering time: 9017 sec.

### 5.3.2 Rendered Flares with Varied Bounce Limits

In our tests we also explored limiting the bounce cutoff for photons within the lens. Photons that exceeded this cutoff were culled. The results show that the majority of the effect is created by photons following a "z-shaped" path, that is, a path containing two reflections. For the light source position in all images, $x = -400$, $y = 66$.

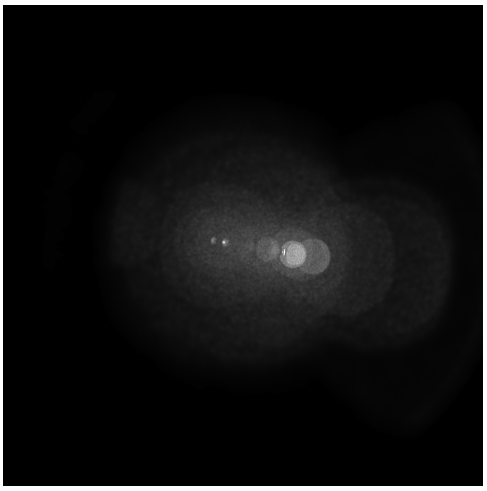

Figure 5.6: This flare was rendered using a bounce limit of 2, and 10 million photons. The flare appears complete despite the low bounce limit.

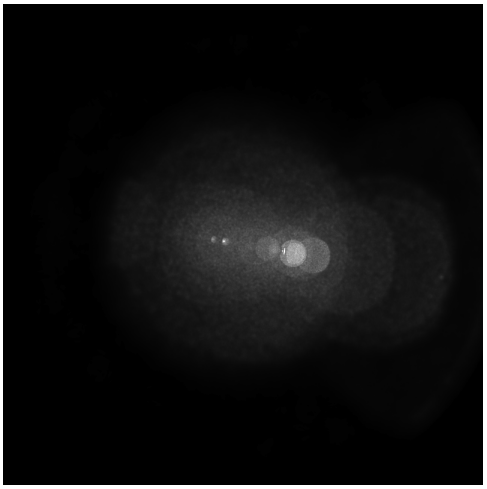

Figure 5.7: This flare was rendered using a bounce limit of 5, and 10 million photons. The flare is comparable to the 2-bounce flare above, and there are no significant visual differences.

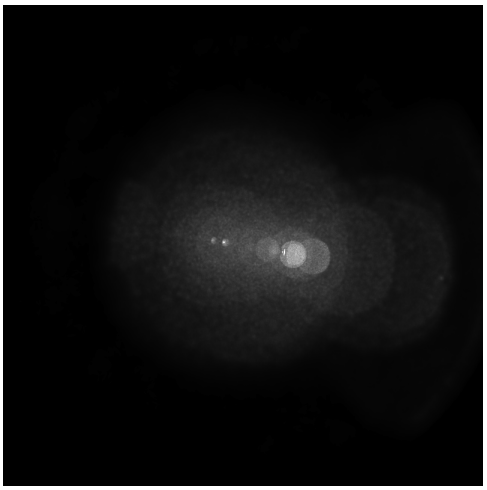

Figure 5.8: This flare was rendered using a bounce limit of 10, and 10 million photons. The flare is still comparable to the 2-bounce flare above, and there are no significant visual differences. We can conclude that the major contributions to the flare come from photons following the 2-bounce "z-shaped" path.

### 5.3.3 Rendered Flares with Massive Photon Quantities

In this subsection we render flares with a large number of photons. These renderings were performed on a variety of Intel Xeon NetBurst machines. The rendertimes were between 12 and 15 hours per image. The results produced are visually more defined than in images with smaller photon quantities.

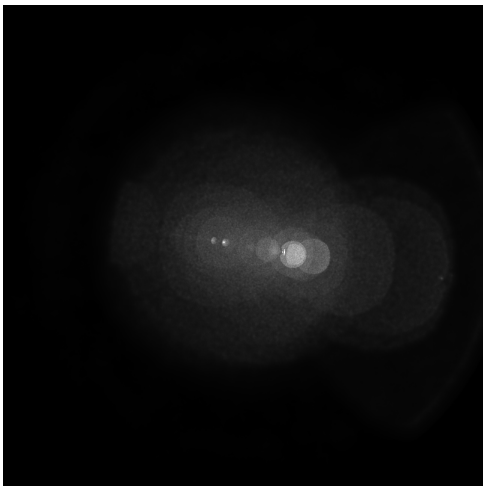

Figure 5.9: This flare was rendered with 20 million photons. For the light position, $x = -400$mm, $y = 66$mm.

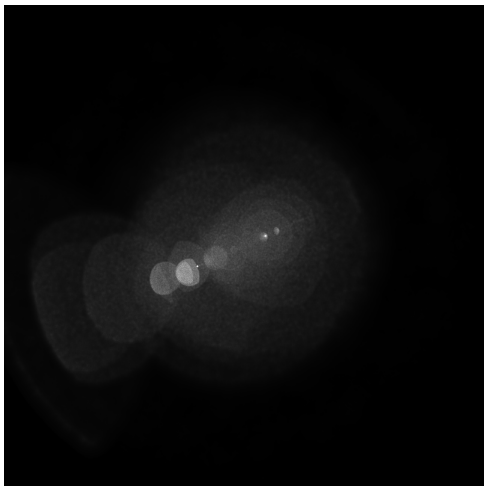

Figure 5.10: This flare was rendered with 20 million photons. For the light position, $x = 450$mm, $y = 200$mm.

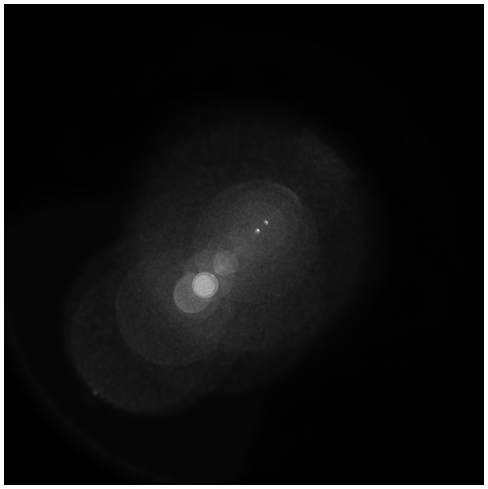

Figure 5.11: This flare was rendered with 20 million photons. For the light position, $x = 300$mm, $y = 300$mm.

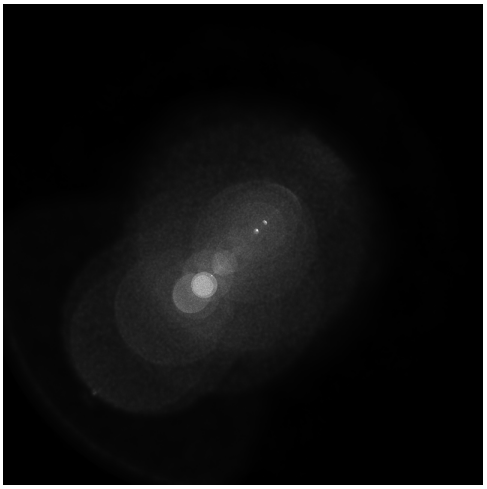

Figure 5.12: This flare was rendered with 20 million photons. For the light position, $x = -400$mm, $y = 66$mm.

## 5.4 Photographic Examples

Due to the difficulty in finding lenses that meet *both* of the following conditions: a) are available to us, and b) have public schematics, we are forced to use real-life approximations for the equipment simulated. To approximate the Nikon 80-200mm $f/2.8$, we use a Canon EF 70-200mm $f/2.8$**L** mounted on the Canon EOS-1Ds Mark I.

### 5.4.1 Canon EF 70-200mm $f/2.8$**L**

This lens was shot at approximately 80mm.

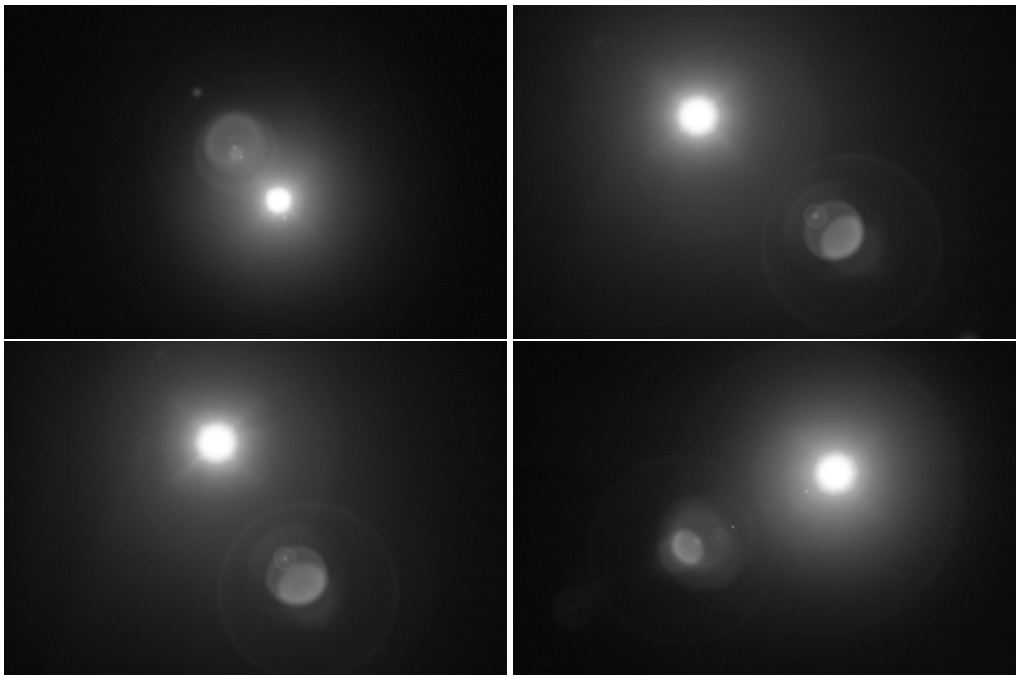

Figure 5.13: Reference flares from the telephoto lens, $f/2.8$.

## 5.5 Discussion of Results

A review of the renderings in the previous sections of this chapter shows the similarity of the circular ghosts rendered with our method and those captured with a real lens. While the lenses are not precisely the same optically, the comparison serves to show that the effect is visually similar, and it is reasonable to expect that the differences in size and position of the circular ghosts between the real and rendered images would be resolved were the same lens used.

The photographs show a few effects that we do not consider in our approach, such as the bloom and glare effect present at the light source, which manifests as streaks and a glow phenomenon. We discuss this in greater detail in Section 4.4. Were these effects not present, the size of the source would appear much smaller in the photographs.

Aside from the rendered images themselves, this technique allows the light path through the lens to be visualized, as in Figure 5.14. The figure shows the ”thickening” of the light beam as it is distributed outwardly by reflections at each interface. Instead of converging as a pure point, the light paths are spread, producing the circular ghosts we see in the renderings. Each ghost is produced by reflections from a specific interface, and as a general rule, ghosts that are produced by reflections spreading the light path away from the image path earlier in the lens system are the ghosts that appear larger in the rendering.

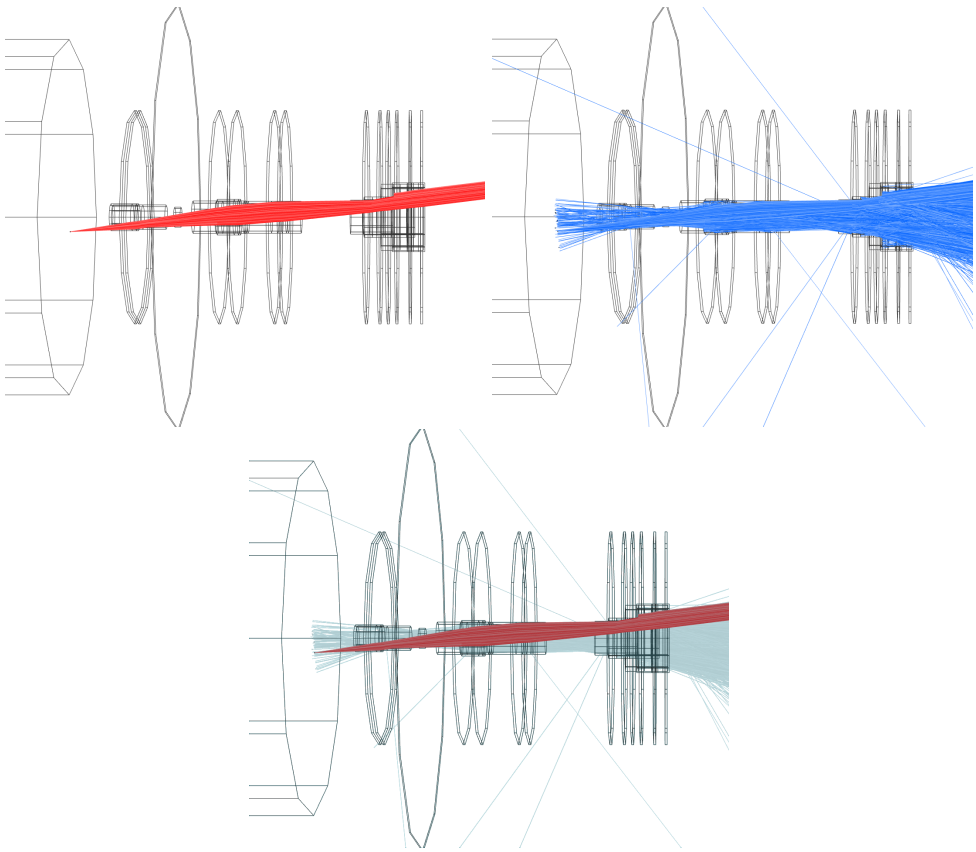

Figure 5.14: Photon paths through the lens system. The elements are shown as cylinders due to limitations in OpenGL rendering of CSG models. The top image shows the image-forming path, with no reflections at any of the interfaces. The second image shows the full behavior, with reflections. The third image is an overlay of the two for comparison.

# Chapter 6.

# Future Work

It is our hope that this thesis provides a foundation for future work in camera simulation. There are many avenues of improvement in both speed and scope. While the rendering of ghost images is fundamental to capturing the appearance of lens flares, there are other phenomena present in flares that must be simulated in order for the effect to be complete. We mention in Chapter 2.1 a few of these phenomena, namely the diffraction effects present at the aperture, as well as the effect of coatings on the color of the circular ghosts. The long render times of our method could stand to be shortened as well. Areas in which the speed of the simulation could be improved are in more efficient methods of casting photons, as this is the main computational bottleneck of our simulation. We expand on future work in these areas in this section.

## 6.1 A Complete Simulation of Lens Flare

### 6.1.1 Wave Effects

The wave nature of light plays an important role in the phenomena present in lens flares. The most visually apparent of these is the star-shaped bloom present in the image at the source of the flare. This flare reveals the aperture

used in the lens, as a five-bladed aperture will yield a five-sided star, a seven-bladed aperture reveals a seven-sided star, and so on. Lenses with circular apertures (such as lenses stopped fully-open) will not have a star at all, but rather a sort of blurry gradation at the source caused by light diffracted by the edge of the aperture. In addition to aperture diffraction, chromatic diffraction effects play a role as well. The glass elements of the lens occasionally contribute streaky rainbows of color caused by chromatic aberrations, and these also lend character to some flares. Many digital sensors themselves also contribute chromatic effects, as the surface of the sensor itself can generate characteristic sensor-flares, which manifest as a faint grid of rainbows over an area of the image.

### 6.1.2 Coatings

Nearly all modern photographic lenses have some form of anti-reflective coating. The physical mechanisms of these coatings are detailed in Section 2.1, and the effect of the coatings on the appearance of the flare are made clear at the beginning of this chapter. The simulation of these coatings is difficult however, for two reasons. The first is that the specifications for many of the coatings used by major lens manufacturers are secret, and the second is that the type of coatings used on the elements of lenses in lens specifications is also not published.

The anti-reflective coatings used by lens manufacturers involve wave-offset interference processes, and so a spectral simulation will be required to adequately model their reflection absorption properties.

## 6.2 Improving the Speed of Lens Flare Simulation

To create the photon map in our simulation we must trace each photon through the elements of the lens and onto the sensor. In addition, a far larger quantity of photons trace partway through the lens and are lost in between el-

ements due to absorption by the sides of the lens. This tracing process is the task which requires the most computational effort in our simulation, and effort expended in reducing the computation required at this stage will greatly benefit the speed of the simulation. Potential improvements in this area could involve schemes such as importance sampling the entry directions on the lens and shooting more photons where they are likely to pass through the lens to the sensor. This method is likely to be quite effective as there is a significant coherency between entry directions. As for the tracing process itself, data structures exploiting the linearity of travel between lens elements will certainly be successful as well. In such a scheme, if a photon is interacting with element four, the next interaction for that photon must be with elements three, four, or five. This greatly limits the number of intersection tests required, and can impose a significant benefit in lenses with many elements. Further still, the direction of travel for each photon can be considered, and an analytical solution may exist to determine the exact next intersection surface in many cases.

# References


Chaumond, J., 2007: Realistic Camera: Lens Flares. Project Webpage: http://graphics.stanford.edu/cs348b-07/JulienChaumond/FinalProject. Final Project for Stanford CSE348B Course.

Franke, G., 1966: *Physical Optics in Photography*. The Focal Press, first edition.

Jensen, H. W., 2001: *Realistic Image Synthesis Using Photon Mapping*. A K Peters, first edition.

Kingslake, R., 1992: *Optics in Photography*. SPIE Publications, second edition.

Kolb, C., Mitchell, D., and Hanrahan, P., 1995: A realistic camera model for computer graphics. *Computer Graphics*, **29**(Annual Conference Series), 317–324.

Koren, N., 2007: Veiling Glare (Lens Flare). http://www.imatest.com.

Marston, P. L., Langley, D. S., and Kingsbury, D. L., 1981: Light scattering by bubbles in liquids or in glass. Technical report, Washington State Univ., Pullman.

Smith, W. J., 2000: *Modern Optical Engineering*. SPIE Press, third edition.

Smith, W. J., 2005: *Modern Lens Design*. SPIE Press, second edition.